
**ISBN number for Chemeca 2020 is 978-1-925627-46-6**

*Chemeca 2020*
*Starting 29 September, Online*

# Transforming the Desorption Unit in Carbon Capture Technology through a Novel Solar-Driven Process

Scott Nelson [1,2], Minh Tri Luu [1], Si Suo [1], Dia Milani [2,*], Ali Abbas [1,*].

[1] School of Chemical and Biomolecular Engineering, The University of Sydney, NSW 2006, Australia

[2] CSIRO Energy Centre, 10 Murray-Dwyer Circuit, Mayfield West, NSW 2304, Australia

snel5915@uni.sydney.edu.au

[*] Dia.Milani@csiro.au

[*] Ali.Abbas@sydney.edu.au

**ABSTRACT**

*Solvent-based post-combustion carbon capture (PCC) as a means of preventing harmful emissions from coal-fired power plants, remains highly relevant to addressing global warming. However, the energy penalty of this retrofit is significant. Therefore, the concept of solar-powered solvent regeneration is proposed to alleviate the reliance on the steam bleeding from the power plant that drives the traditional PCC process. We present a solar field pipe network to replace the conventional and costly desorption unit. This pipe network consists of modular "solar-strippers" (So-St) that function to regenerate the rich solvent and desorb the $CO_2$ gas to be vented out of the loop. The regenerated solvent becomes lean and is recycled back to the absorber. The So-St exhibits fluid phenomena distinct from a conventional desorber, with design complexity that is best dealt with by computational fluid dynamics (CFD) when targeting enhanced desorption efficiencies. This study develops a CFD model for a single So-St segment; the first of its kind. The design is investigated in terms of boiling flow, multi-phase evolution, fluid regimes, heat transfer, reaction kinetics and thermodynamics. A preliminary model in 2-D is evaluated and divided into two segregated sub-models to assess the chemical compositions and phase development along the So-St tube. The results of this model provide a comprehensive insight on this unique two-phase evolving flow that can help in developing a more accurate 3-D model and consequent design of the So-St system. It is found that implementing enhanced heat transfer (EHT) methods is essential for increasing the So-St efficiency and eventually reducing the solar field size.*

***Keywords:*** Post-combustion carbon capture; energy penalty; desorption; solvent regeneration; solar energy; computational fluid dynamics.

## INTRODUCTION

The mitigation of global warming is becoming increasingly urgent, as the goals of the 2015 Paris climate agreement are becoming more difficult to achieve (Figueres et al., 2017). Fossil-fuel fired power plants (PPs) account for approximately 64% of the world's electricity generation (BP, 2020), and are one of the main contributors to the $CO_2$ emissions, the most harmful greenhouse gas (IEA, 2013). Carbon capture and storage (CCS) technologies are well-recognised as having an essential role in offsetting global warming by capturing and processing the $CO_2$ for sequestration or utilisation (Wilberforce et al., 2019). This technology has received much support from the Intergovernmental Panel on Climate Change (Rubin et al., 2005) and the International Energy Agency (Taylor, 2010), the latter estimated the CCS to account for up to 19% of the global emission reductions by 2050.

Post-combustion carbon capture (PCC), when compared to the other available CCS methods (pre-combustion and oxy-fuel combustion), appears most promising for commercial application (Duke et al., 2010). This is primarily due to its downstream implementation, making it suitable to target mature, existing coal-fired PPs, without the need for costly modification to the plant itself. Solvent-based PCC functions through an absorption-desorption cycle where $CO_2$ is absorbed from the flue gas of a PP into a lean solvent, typically amine-based solvents such as monoethanolamine (MEA) (Mumford et al., 2015). The subsequent rich solvent (saturated with $CO_2$) is then heated in a desorber column to separate $CO_2$ gas for further processing, allowing the regenerated lean solvent to be recycled back to the absorber. Solvent-based PCC has been of significant interest over other PCC technologies, such as physical adsorption (Ben-Mansour et al., 2016), membranes (Khalilpour et al., 2015) and mineralisation processes (Zevenhoven et al., 2009). This is due to its large-scale reliability, maturity in the research field, and the ease of achieving both process conditions and absorber retrofitting (Aaron et al., 2005). The main obstacle hindering solvent-based PCC practicality in industry is its significant energy penalty (Feron, 2009). The process requires large thermal energy for solvent regeneration in the desorber and electricity for auxiliary equipment, such as pumps and compressors. When this energy is bled from the PP, it leads to a reduction in efficiency by 19.5 – 40% (Parvareh et al., 2014), making its current economic viability insufficient to be a desirable investment for plant owners.

Solar-assisted PCC (SPCC) has been investigated to compensate for the loss in energy productivity, by introducing renewable solar energy, particularly sourced from solar thermal collectors (STCs) (Saghafifar et al., 2019). For example, SPCC can directly supplement the reboiler energy of the desorber using a working fluid, such as steam, to lower the intensive energy requirements (Wibberley, 2010). This direct method has ease of implementation, however an inherent limitation is the solar energy having to pass through multiple heat transfer media which lowers the thermal efficiency. SPCC may also be used indirectly via integration with the PP itself, where energy is supplemented within the power station cycle (Zhao et al., 2012). Although this has shown promise in offsetting the energy penalty and reducing levelised solar field costs, it requires modification to the power plant operation itself, making it targeted towards new PPs, rather than those which are already existing and mature. Furthermore, SPCC hasn't been a commercially viable solution primarily due to the solar intermittency and the costly thermal energy storage (TES) when solar energy is unavailable (Qadir et al., 2013).

In the interest of developing novel SPCC technologies which are non-invasive to the PP, Khalilpour et al. proposed a concept of solar-assisted solvent regeneration which eliminates the desorber system (Khalilpour et al., 2017). A redesign of the desorber was proposed, which would rely solely on energy from a solar collector field (SCF) to heat, strip and regenerate the rich solvent as a working fluid directly within the SCF receiver tubes. A solvent storage system was also recommended as a buffer which accounts for solar intensity changes throughout the day/night and yearly seasonal variations. Advantages for this process are seen in the lower heat losses due to less heat transfer media (e.g. no steam working fluid); elimination of the desorber system which is estimated to account for 15-30% (Abu-Zahra et al., 2007; Manzolini et al., 2015) of the total capital costs; reduction of operating costs due to less maintenance and higher energy efficiencies. Moreover, the desorber unit often requires regeneration energies larger than theoretical values resulting in excess steam demand. This proposal would reduce the complexity of the solvent regeneration process by making it independent from the

power-plant steam cycle and will enable higher flexibility for energy market dynamics.

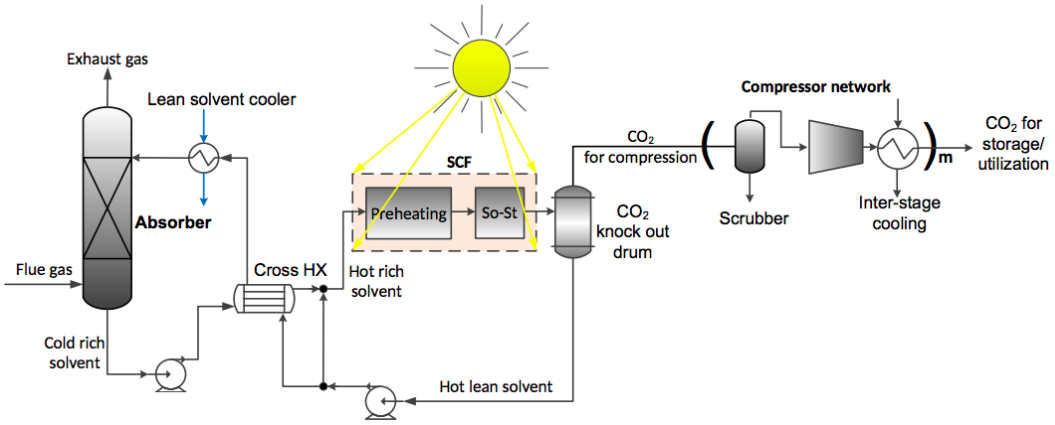


**Figure 1: Division of SCF desorption process into a preheating section and a solar stripper. Recreated from (Milani et al., 2020).**

Milani et al. further investigated this concept and separated the SCF desorption process into two key functions: (1) a pre-heating section achieved using appropriate solar technology to heat up the rich solvent to the targeted temperature for desorption (~120°C), and (2) the solar stripper (So-St) being a custom designed pipe network to replace the desorber system, using concentrated solar power to directly break $CO_2$-solvent bonds and release $CO_2$ from the solvent (Milani et al., 2020a) (Figure 1). The $CO_2$ gas can then be separated from the solvent at the end of or intermediately within the So-St network using a flash drum. The initial work focused primarily on the pre-heating section, undertaking a case study with weather data from three different solar zones in Australia over a year, with the purpose of capturing 1.5 million $tonne_{CO2}$/y from a 660 $MW_e$ coal-fired power plant. The study showed the SCF sizing necessary to pre-heat the rich solvent up to the critical temperatures for desorption, along with the use of solvent storage tanks to buffer the effects of daily and seasonal solar variations.

Despite the promising results regarding the first key function of pre-heating, it is essential to investigate and develop a working design for the second key function, namely the So-St. Although the So-St has the same theoretical function as a conventional desorber, a major design revaluation is necessary to account for its novel energy source derived from the direct heating of concentrated solar thermal collectors (STCs). Various new design constraints are in effect, for example: solar collector absorber tubes typically have diameters of ~70 mm (e.g. Schott PTR80 – 76 mm; Solel UVAC 3 – 66 mm). In a conventional desorber, the vessel diameters are on the order of 5 m (Moresa et al., 2011). Furthermore, the heat transfer in a desorber occurs only within the reboiler at the bottom of the vessel, whereas a solar collector will distribute heat along the entire length of the receiver tube according to a non-uniform distribution (Cheng et al., 2012). The desorber vessel also has two-phase flow along a vertical axis, whereas the SCF receiver tubes are predominantly horizontal, with scope for tilting according to the SCF topography.

Milani et al. established the first working So-St model using Aspen® software (Milani et al., 2020b). Parabolic trough collectors (PTCs) were chosen as the STC application for the So-St. PTCs have highly concentrated solar input, which is essential to meet the high energy requirements for desorption, despite the relatively higher capital cost of PTCs compared to other non-concentrating STCs (Li et al., 2012; Qadir et al., 2013). Considering that the design will process large flowrates of rich solvent, the So-St was modularised, where individual and identical So-St segments would be constructed and combined together both in parallel and in series, to ensure $CO_2$ capture efficiency and volume targets are met. The study customised and optimised the length and diameter of a single So-St segment and determined the So-St field size with its corresponding number of segments and modules.

Currently, the So-St segment has only been investigated through the lens of a black-box model, which relates inputs and outputs without considering the internal geometry of the design. Although geometry and sizing for the So-St have been proposed to meet the PCC design target for the case-study (1.5 million $tonne_{CO2}$/y from a 660 $MW_e$ coal-fired PP), the previous modelling approach assumes complete transfer of heat and that the system operates at the thermodynamic design point. This

method has value for computational simplicity, however has limitations in accuracy, for example the solar heat profile for PTCs is non-uniformly distributed around the receiver tube (Cheng et al., 2012), which may promote local hotspots and eventually impact the overall flow and heat transfer behaviour. Other phenomena, such as temperature gradients may form due to heat accumulating near the tube surface. These gradients may impact the boiling flow regime and can be detrimental to the physical properties of the MEA solvent, which is reported to undergo thermal degradation at temperatures > 125°C at a conventional desorber pressure of 1.6 atm (Davis et al., 2009). It is essential to develop a model which accurately describes the thermochemical events inside the So-St tube, so that its performance can be evaluated to a greater accuracy. A model as such has further implications for determining methods of improving $CO_2$ removal to enhance the So-St capability, such as via heat transfer augmentation techniques (Sandeep et al., 2017).

As the solvent flows inside a solar receiver tube, a portion of the liquid is vaporised and the $CO_2$ molecules are eventually released. The vapour molar fraction (VMF) of the flow gradually increases along the length of the receiver tube, and subsequently, different flow regimes would evolve (Figure 2). Describing this very complex physico-chemical process mathematically under transient conditions is a very challenging task. The asymmetrical solar heat profile around the tube cross-sectional area adds more complexity to predict vapour phase evolution and flow regime along the receiver tube, which may require robust and intensive modelling. Adding more complexity is the unknown extent of the desorption chemical reactions on various species compositions under these transient conditions. Computational fluid dynamics (CFD) offers an attractive method of exploring the internal complexities of a So-St segment and its fluid phenomena. The So-St carries complex physical phenomena, in particular boiling flow, which is a problem commonly solved using CFD (Kharangate et al., 2017). Previously, multi-phase boiling flow has been modelled within PTC receiver tubes primarily for the purpose of steam generation (Lobón et al., 2014a; Lobón et al., 2014b; Yerdesh et al., 2018), however this current study is interested in a CFD model formulation that is specific to the So-St tube geometry and design specifications. CFD has also been used in PTCs to assess the capabilities of enhanced heat transfer (EHT) methods, which entail the addition of inserts or tubes with surface augmentation (Yılmaz et al., 2018). For the So-St, CFD may reveal designs that enhance $CO_2$ removal.

This study details the construction of a CFD model, using the COMSOL Multiphysics package, to understand the internal design of a single So-St segment. The So-St is evaluated in terms of heat transfer, vapour formation, flow development and $CO_2$ concentrations. Here, the preliminary results for the So-St tube are presented for the bare So-St tube, without internal modification. However, these results display the need for a detailed analysis into EHT methods which have potential to enhance the So-St performance by increasing heat transfer and ultimately improving the $CO_2$ removal efficiency. The CFD modelling enables the So-St process to become an economical and efficient method for $CO_2$ desorption, that eliminates the reliance on the power plant steam cycle.

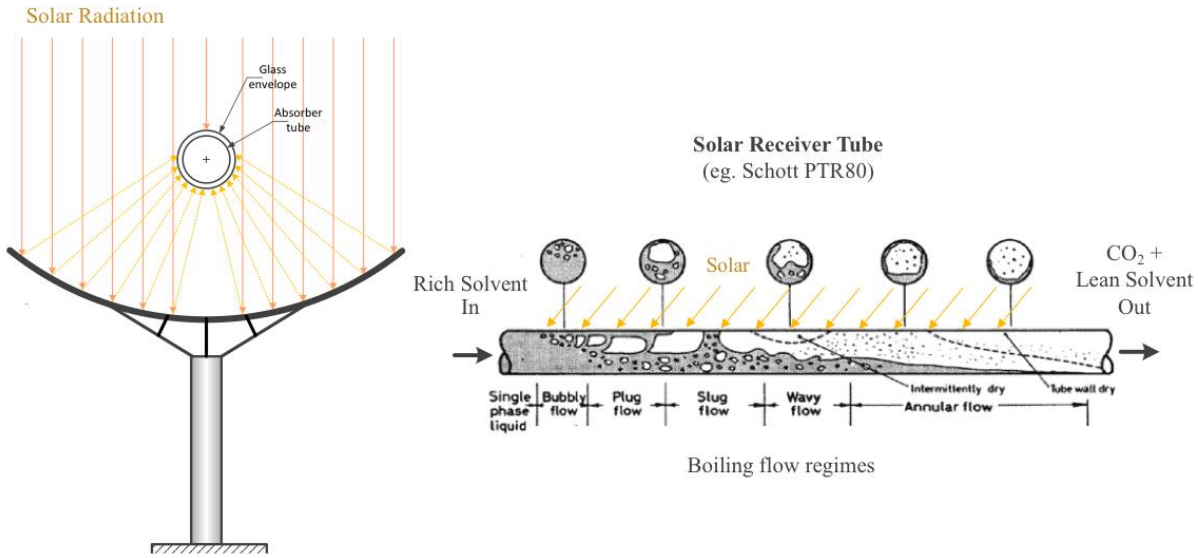


**Figure 2: The solvent passes through the solar receiver tube of the parabolic trough collectors. Computational fluid dynamics is used to investigate boiling flow regime and optimise heat transfer as a function of solar heat availability. Pipe flow diagram recreated from (Collier & Thome, 1994).**

## MODELLING METHODOLOGY

CFD modelling of the So-St segment is conducted using the COMSOL Multiphysics package. Because CFD modelling generally requires significant computational time/power, it is of interest to reduce the computational load, such as by limiting the range of simulation time, tube length and mesh size, without compromising the model accuracy. In this work, it was decided to explore the So-St segment in a 2-D geometry. This is characterised by a rectangular cross-section along the length of the tube, with the height corresponding to the tube diameter and gravity defined along the vertical axis. Compared to a 3-D pipe model, the 2-D pipe model is less accurate since it does not account for flow across the third dimension and the heat transfer which occurs along the sides of the pipe. However, it is an essential step to provide significant insight on the solvent thermo-physical properties without compromising on the computational time/power. The 2-D model results will then be analysed to inform the decision making process in the more advanced 3-D model.

CFD modelling is conducted in COMSOL using the finite volume method (FVM) which discretises the entire spatial domain into a mesh of small control volumes. The key design parameters for the So-St are displayed in Table 1.**Error! Reference source not found.** The COMSOL Multiphysics package is ideal for describing the So-St design, which incorporates a wide range of important physical phenomena, namely heat transfer, thermodynamics, multi-component chemical reaction, fluid flow and multiphase evolution. However, it is a challenge in CFD at large to couple all five physical phenomena into a single model. This is due to the difficulty to dynamically track the gas-liquid frontier, as it acts as an interface for multi-species diffusion between the two phases. This problem is yet to be resolved by the CFD developers' community, to the author's knowledge, and thus a compromise was made by decoupling the phenomena into two distinct sub-models. The multi-species and chemical reaction are coupled together in the first sub-model. This sub-model is in single-phase and excludes the evolution of a gas-liquid interface, whilst describing heat transfer, flow behaviour and chemical reactions with the presence of water, $CO_2$, and MEA components. The second sub-model couples hydrodynamics and interface evolution, and is performed in multi-phase yet in a single-component water-only scenario, excluding all other chemical species and reactions. Although the assumption of single-component strays from the real scenario, the concentrations of MEA and $CO_2$ components are dilute and thus the formation of water vapour phase is used as an analogy to that of the $CO_2$ gas evolution. The single-component model therefore enables an evaluation of the So-St in its ability to promote vapour phase evolution, and hence $CO_2$ removal. The heat transfer module is utilised in both sub-models, being a necessary driving force for both chemical reaction and vapour

evolution. The proposed modelling framework allows the So-St to be evaluated for the physical phenomena separately, and the conclusions from both sub-models can be integrated to inform methods through which the So-St performance can be improved.

**Table 1: Key design parameters for a So-St tube.**

| Design Parameter | Value | Unit |
|---|---|---|
| So-St length | 2 | m |
| So-St diameter (inner/outer) | 76 / 81 | mm |
| Operating pressure (inlet) | 2 | bar |
| Inlet temperature | 120 | °C |
| Inlet velocity | 0.3 | m/s |
| Rich loading | 0.4 | $mol_{CO2}$ / $mol_{MEA}$ |
| Lean loading target | 0.3 | $mol_{CO2}$ / $mol_{MEA}$ |

**Sub-Model 1 - Chemical Reaction**

Sub-Model 1 investigates the So-St tube in purely liquid phase and includes the $CO_2$ and MEA components and their corresponding reactions. This investigation has implications for evaluating gradients in temperature, velocity and pressure, and is highly relevant in determining fluid behaviour before the So-St boiling flow has begun. The So-St model geometry consists of a 2m × 0.076m rectangular cross-section, corresponding to the tube length and diameter, respectively. The model was run for a simulation time of 10 s.

The fluid flow is assumed incompressible and Newtonian, and the Reynolds-averaged Navier Stokes (RANS) equations are used, as seen in Equations 1 and 2.

$$\rho\frac{\partial \boldsymbol{U}}{\partial t}+\rho\boldsymbol{U}\cdot\nabla\boldsymbol{U}+\nabla\cdot\left(\overline{\rho\boldsymbol{u}'\otimes\boldsymbol{u}'}\right)=-\nabla P+\nabla\cdot\mu(\nabla\boldsymbol{U}+(\nabla\boldsymbol{U})^{T})+F \qquad (Eq.1)$$

$$\rho\nabla\cdot\boldsymbol{U}=0 \qquad (Eq.2)$$

where $\rho$ is the density (kg/m$^3$), $\boldsymbol{U}$ is the averaged velocity field, $\boldsymbol{u}$ is the velocity vector (m/s), $\otimes$ is the outer vector cross product, $\mu$ is the dynamic viscosity (Pa s).

The turbulent flow *k-ω* model is used to solve the RANS equations. This involves solving the turbulent kinetic energy ($k$) equation (Equation 3) and the specific dissipation rate (ω) equation (Equation 4). COMSOL uses the Wilcox revised *k-ω* model (Wilcox, 2008).

$$\rho\frac{\partial k}{\partial t}+\rho\boldsymbol{u}\cdot\nabla k=P_k-\rho\beta^{*}k\omega+\nabla\cdot\left(\left(\mu+\sigma^{*}\mu_T\right)\nabla k\right) \qquad (Eq.3)$$

$$\rho\frac{\partial \omega}{\partial t}+\rho\boldsymbol{u}\cdot\nabla\omega=\alpha\frac{\omega}{k}P_k-\rho\beta\omega^{2}+\nabla\cdot\left((\mu+\sigma\mu_T)\nabla\omega\right) \qquad (Eq.4)$$

where $P_k$ is the production of turbulence kinetic energy; $\mu_T$ is the eddy viscosity; $\alpha, \beta, \sigma$ are closure coefficients for the specific dissipation rate equation; $\beta^*, \sigma^*$ are closure coefficients for the turbulent kinetic energy equation. The heat transfer interface is utilised which solves the heat equation in Equation 5.

$$\rho C_p\frac{\partial T}{\partial t}+\rho C_p\boldsymbol{u}\cdot\nabla T=\nabla\cdot(k\nabla T)+Q \qquad (Eq.5)$$

where $C_p$ is the specific heat capacity at constant pressure (J/kg/K), $T$ is the absolute temperature (K), $k$ is the thermal conductivity (W/m/K), and $Q$ refers to heat sources other than viscous heating (W/m$^3$). A limitation for modelling PTC tube flow in 2-D is the difficulty to appropriately resolve the PTC heat flux distribution. Heat transfer for the PTC is at a constant heat flux boundary condition, which is non-uniformly distributed around the tube circumference of the tube. For a 3-D model, it is natural to define this heat distribution profile around the circumference according to the local solar concentration ratios. However, the 2-D cross-section is an infinitesimal width and the boundary conditions can only include heat transfer from the top and bottom edges of the cross-section. The

direct top and bottom of the PTC are not the areas of highest solar concentration; the maximum occurs at angle incline of ~100° (Cheng et al., 2012). It is important to have an appropriate heat transfer driving force which is not solely defined by the top and bottom surfaces of the tube. To resolve this issue, we instead set the heat transfer boundary condition to be a constant surface temperature, rather than a constant heat flux. Using previous Aspen modelling results, we find a constant surface temperature of 140°C to create an equivalent heat flux to that of the constant heat flux boundary condition. Thus, the surface of the So-St tube is assumed to be 140°C. The transport of diluted species interface is utilised in COMSOL. The mass transport of species ($H_2O$, $CO_2$, MEA and ionic species) between control volumes is governed by diffusion and convection which are driven by concentration and pressure gradients respectively, according to the following mass balance equation:

$$\frac{\partial c}{\partial t} + \boldsymbol{u} \cdot \nabla c = \nabla \cdot (D \nabla c) + R \qquad (Eq.6)$$

Where $c$ is species concentration (mol/m$^3$), $D$ is the diffusion coefficient (m$^2$/s), and $R$ is the reaction rate expression for the species (mol/m$^3$/s).

The chemistry associated with $CO_2$ absorption/desorption in MEA solution can be described with the following set of reactions:

Overall reaction of MEA and $CO_2$

$$CO_2 + 2MEA \overset{K_{eq,1}}{\longleftrightarrow} MEACOO^- + MEAH^+$$

Carbamate reversion to bicarbonate

$$MEACOO^- + H_2O \overset{K_{eq,2}}{\longleftrightarrow} MEA + HCO_3^-$$

MEA deprotonation

$$MEAH^+ + H_2O \overset{K_{eq,3}}{\longleftrightarrow} MEA + H_3O^+$$

Bicarbonate formation

$$CO_2 + 2H_2O \overset{K_{eq,4}}{\longleftrightarrow} HCO_3^- + H_3O^+$$

Dissociation of water

$$2H_2O \overset{K_{eq,5}}{\longleftrightarrow} OH^- + H_3O^+$$

For reactions 2 to 6, the equilibrium constants defined according to Equation 7.

$$K_{eq} = \frac{A^a B^b}{C^c D^d} \qquad (Eq.7)$$

where $A$ and $B$ are the molar concentration of products (mol/m$^3$); $a$ and $b$ are the stoichiometric ratios of the products; $C$ and $D$ are the molar concentration of reactants (mol/m$^3$); $c$ and $d$ are the stoichiometric ratios of the reactants. Thus, the equilibrium constant for the overall reaction between MEA and $CO_2$ can be written in terms of the other equilibrium constants, as seen in Equation 8.

$$K_{eq,1} = \frac{K_{eq,4}}{K_{eq,3} K_{eq,2}} \qquad (Eq.8)$$

**Sub-Model 2 - Hydrodynamics and Interface Evolution**

Sub-Model 2 is used to investigate the vapour formation within the So-St. The sub-model includes water as a single component. The neglected $CO_2$ and MEA species simplifies the process, and is a reasonable assumption considering that these chemical components are much diluted compared to the water component. The vapour phase behaviour for the single-component water is therefore used as an analogy for comparison to the actual phenomenon, since $CO_2$ molecules leaving the solution concurrently with the water molecules. To model the interface evolution, a separated multiphase model is utilised, which dynamically tracks the gas-liquid interface and its evolution across the tube using the phase field method. The method is ideal for smaller-scale models and has greater accuracy

compared with dispersed phase models.

For gas-liquid flow, the liquid phase is characterised by the incompressible Navier-Stokes and continuity equations, whilst the gas phase is characterised by the compressible Navier-Stokes and continuity equations.

$$\nabla \cdot \boldsymbol{u} = 0 \qquad (Eq.9)$$

$$\frac{\partial(\rho \boldsymbol{u})}{\partial t} + \nabla \cdot (\rho \boldsymbol{u}\boldsymbol{u}) - \nabla \cdot (\mu \nabla \boldsymbol{u}) - \nabla \boldsymbol{u} \cdot \nabla \mu = -\nabla p + F_{st} + F_{ext} \qquad (Eq.10)$$

The phase field method is characterised by the Cahn-Hilliard diffusion equation (Equation 13), which introduce the dimensionless phase field variable $\boldsymbol{\varphi}$, where the pure liquid phase is $\boldsymbol{\varphi}$ = 0 and pure vapour phase is $\boldsymbol{\varphi}$ = 1.

$$\frac{\partial \phi}{\partial t} + \boldsymbol{u} \cdot \nabla \phi = \nabla \cdot \frac{\gamma \lambda}{\epsilon^2} \nabla \psi \qquad (Eq.13)$$

$$\psi = -\nabla \cdot \epsilon^2 \nabla \phi + (\phi^2 - 1)\phi + \left(\frac{\epsilon^2}{\lambda}\right)\frac{\partial f}{\partial \phi} \qquad (Eq.14)$$

$$\lambda = \frac{3\epsilon\sigma}{\sqrt{8}} \qquad (Eq.15)$$

where $\psi$ is the auxiliary variable, $\epsilon$ is the capillary width, $\lambda$ is the mixing energy density, $\sigma$ is the surface tension, $\gamma$ is the mobility. The heat transfer interface is similarly governed by the heat equation, seen previously in Sub-Model 1 (Equation 5).

The phase field model is constructed using the COMSOL Multiphysics package and is used to model the So-St tube as a 2-D rectangular cross-section, as similar to Sub-Model 1. Similar geometry and boundary conditions are utilised, where the tube cross-section is 2 m × 0.076 m, the liquid inlet temperature is 120°C, and the surface temperature is constant at 140°C. However, a different boundary condition is defined for the phase field model, being a pressure difference constraint between the inlet and outlet of the tube, instead of defining a constant inlet velocity. This pressure drop is defined as 1000 Pa, chosen to reflect the pressure drop seen in previous Aspen modelling over 2 m of So-St tube length. This alteration was chosen since a constant inlet velocity for boiling flow has greater potential for creating back-flow and unstable conditions, which cause convergence issues in the models. In Sub-Model 2, the inlet velocity is therefore a function of time. Additionally, the velocity of flow is set to zero as an initial condition, and the velocity will increase according to the pressure drop constraint and the evolution of vapour. Because the phase field method introduces a considerable computational load, the simulation time was reduced to 2 s, instead of the 10 s simulation time used in Sub-Model 1.

## RESULTS AND DISCUSSION

Sub-Models 1 and 2 were simulated for the So-St tube to display the fluid behaviour under liquid phase and gaseous-liquid phases, respectively. In reality, the So-St will function dynamically throughout the day, and will alternate between single-phase and multi-phase responding to the solar availability. Sub-Model 1 therefore gives insight into the flow behaviour in the initial start-up conditions shortly before vapour evolution is achieved, whereas Sub-Model 2 shows the fluid behaviour at ideal process conditions during $CO_2$ removal.

For Sub-Model 1, the key distributions for temperature, pressure, velocity and $CO_2$ loading are displayed in Figure 3 at the final time step (10 s). Being simple pipe flow in liquid phase, the distributions are smooth with steady behaviour, despite the flow being in a turbulent regime (Re = 9938 > 4000). In the temperature distribution, the hot regions accumulate at the top and bottom surfaces which are at a constant temperature of 140°C. However, these regions are not significantly hot, indicating very minimal heat transfer has occurred between the hot surface and the bulk fluid. This is characterised by the temperature scale ranging between 120 – 122°C and only showing minor temperature gradients near the surface, while the bulk fluid near the radial centre of the tube remains close to 120°C. The low heat transfer is a result of boundary layer formation at the surface.

Furthermore, there is no vertical mixing of the fluid to disrupt this boundary layer, as seen in the velocity profile, the fluid flows parallel to the tube at a constant velocity of 0.3 m/s. For the pressure profile, there is a negligible pressure drop along the tube length and the pressure differences along the vertical direction are a result of gravity. The $CO_2$ loading also remains relatively uniform along the tube length. The overall insight from Sub-Model 1 is that there is much scope for the So-St tube to be improved in its heat transfer performance. Because the So-St must heat up the liquid at the start of the day to reach ideal operating conditions, there is a great benefit for introducing EHT methods which can increase the thermal convection and speed up the start-up process. This can allow a wider operating period throughout the day, which can reduce the load on the large solar field size as a means of achieving the $CO_2$ capture targets.

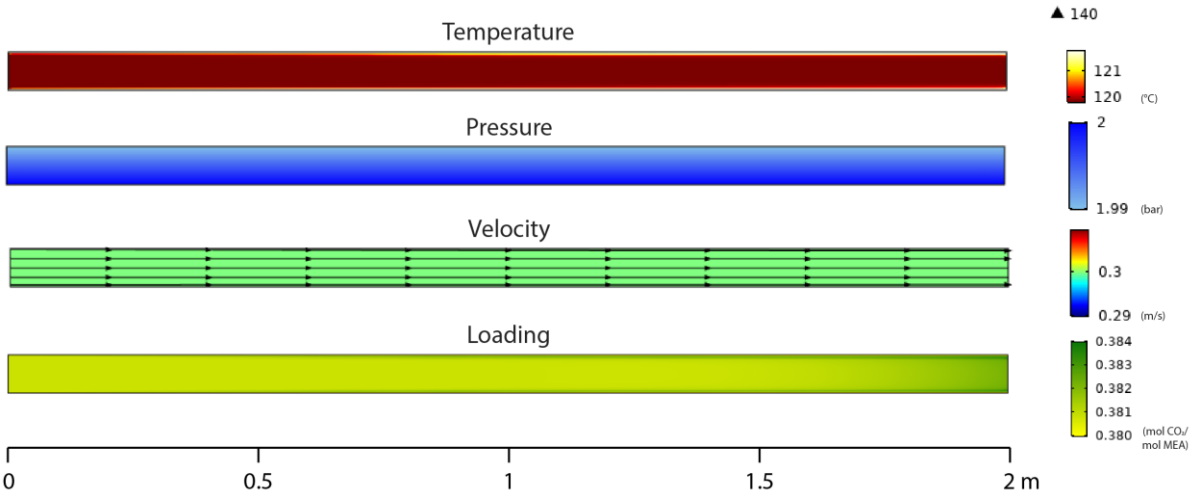


**Figure 3: Sub-Model 1 distributions for temperature (°C), pressure (bar), velocity (m/s) and $CO_2$ loading ($mol_{CO2}$ / $mol_{MEA}$) at final time step of 10 s.**

The Sub-Model 2 simulation displays much more diverse fluid behaviour, due to its multi-phase flow. The phase field method allows the vapour phase to be tracked dynamically along the length of the So-St tube. These distributions are displayed at 0.5 s intervals in Figure 4, showing both bubble formation and phase development. In the first 0.5 s, the nucleation of small bubbles occurs along the bottom side of the tube, which continues throughout the simulation time. By 1.0 s, a stratified flow is generated between the vapour and liquid, where the vapour phase accumulates along the top of the tube due to buoyancy forces. The volume of vapour phase across the entire tube increases with time and a small gradient in liquid fraction is observed between the inlet and outlet of the tube, where the liquid level decreases along the tube length. These gradients have great importance in the design of the So-St modules since the gaseous phase must be periodically vented out from the solvent. This venting process is necessary to maintain the driving force for gas/vapour removal and to prevent dry-out conditions, which can cause damage to the PTC (Kalogirou, 1996). The vapour behaviour suggests prospects for future studies to systematically optimise the locations of vapour removal along the So-St network. The formation of larger bubbles is seen at the inlet of the 1.5 s and 2.0 s intervals. A longer simulation time will be necessary for investigating the behaviour of these larger bubbles downstream, and whether they are a product of inlet behaviour or will form consistently along the tube.

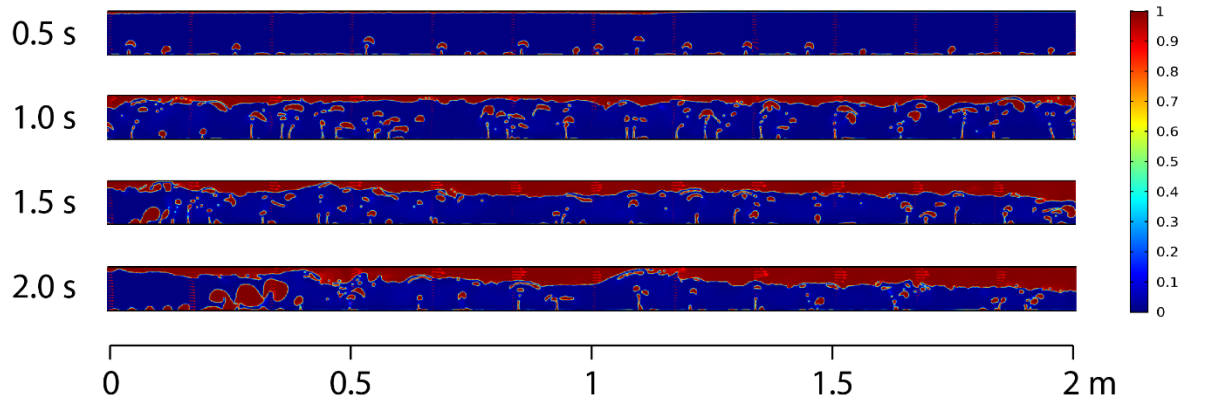


**Figure 4: Vapour fraction distribution over 2 m of tube within So-St over 2 s simulation at 0.5 s intervals.**

The Sub-Model 2 distributions for temperature, pressure and velocity are displayed in Figure 5 at the final time step (2 s), which can be directly compared with the Sub-Model 1 results in Figure 3. The distributions evidently differ between the two Sub-Models. Here in Sub-Model 2, there is much greater distribution of heat within the tube. For example, there are high temperature regions at the top of the tube corresponding to the vapour phase which accumulates there (Figure 5). It must be noted the liquid phase is at saturation temperature, so all energy input is consumed as latent heat rather than sensible heat. The bubbling flow also increases the heat transfer by favouring the vertical mixing within the tube. This is seen in the velocity profile which is highly random and non-uniform with irregular vertical mixing behaviour (Figure 5). Near the entrance region, there are various temperature hot spots; these correspond to the large bubbles seen in Figure 4. Ideally, the heat transfer objective in the So-St is for the fluid to overcome the latent heat of vaporisation, and the heat of $CO_2$ removal in the real-life system. The hot bubble spots however indicate that heat is being utilised for specific heat capacity of the gaseous phase. There may be a need to increase mixing within the So-St tube using EHT inserts, to minimise these large temperature spikes and to favour vapour formation.

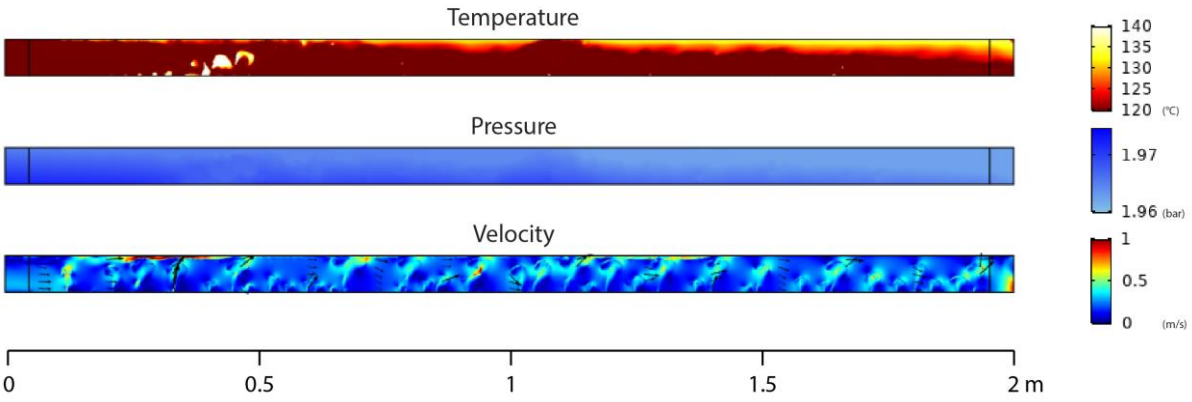


**Figure 5: Sub-Model 2 distributions for temperature (°C), pressure (bar), and velocity (m/s) at the final time step of 2 s.**

The pressure distributions for the sub-models have similar trends in the vertical differences due to the gravity, yet they differ as a result of Sub-Model 2 defining a constant pressure drop (1000 Pa), whereas Sub-Model 1 defines a constant inlet velocity (0.3 m/s) which leads to negligible pressure drop. The pressure drop condition in Sub-Model 2 further creates a dynamic velocity profile. Figure displays the inlet velocities for both sub-models along the simulation time of 2s. For Sub-Model 2, the velocity increases steadily with time. The fluid flow begins at a stationary velocity according to the initial time step condition, and it increases to a maximum of ~0.6 m/s. In the initial time steps, some of this increase in velocity is due to the pressure drop boundary condition favouring fluid flow. However, the behaviour is predominantly a result of the bubble formation creating an expansion in volume that allows the fluid to flow at a greater velocity for the same pressure drop condition. The alternative boundary conditions can be evaluated from a process control perspective. A constant inlet

velocity may be easy to control in single-phase, yet is more difficult in multi-phase due to the inconsistent densities and volumetric flow rates. However, a constant pressure drop is generally more difficult for control. This would certainly entail an advanced process control scheme to monitor the solvent temperature/pressure and provide appropriate remedy control actions for such a novel process.

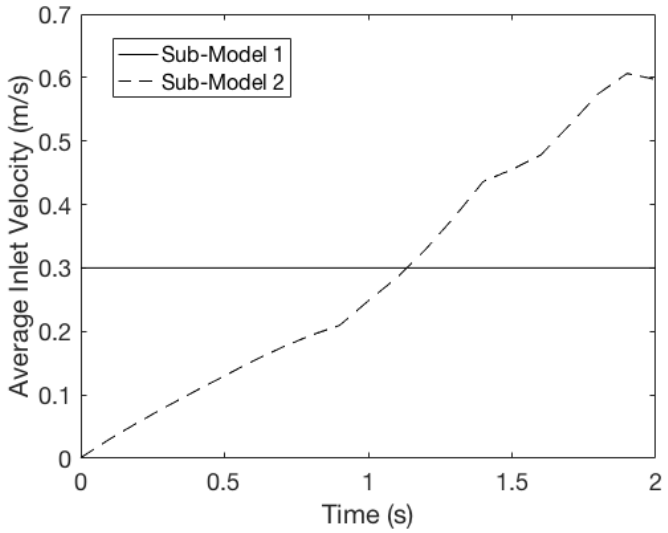


**Figure 6: Average inlet velocity (m/s) for Sub-Models 1 and 2, where Sub-Model 1 entails a constant velocity boundary condition and Sub-Model 2 entails a constant pressure drop boundary condition.**

## CONCLUSION

A novel method of solar-powered PCC was investigated through a CFD study, to address the energy penalty problem for solvent-based PCC technology by aiming at increasing the energy self-sufficiency of the desorption unit using a so-called "solar stripper" or So-St. In the interest of analysing the internal workings of the So-St design, a CFD model using the COMSOL Multiphysics package was constructed to understand the complex flow behaviour. Two sub-models were formulated: (1) a single-phase multi-species chemical reaction model, and (2) a multi-phase single-species phase field model, enabling an integrated analysis of the flow behaviour within the So-St. Sub-Model 1 displayed highly stable flow within the So-St tube before the evolution of vapour, however the significant differences between surface and bulk fluid temperature support the need for implemented methods of enhanced heat transfer. Sub-Model 2 showed the successful vapour phase formation within the So-St tube, however the introduction of internal geometries such as inserts or surface augmentations may be necessary to prevent large bubble formations that have larger temperature gradients and can compromise fluid stability. These preliminary results for the internal workings of the So-St, strengthen the need for enhanced heat transfer methods to improve thermal efficiency and enhance $CO_2$ removal. Further study into these methods will be essential, having direct implications for reducing the load on the solar field size as a means of ensuring $CO_2$ capture targets are met, with potential to reduce the So-St tube length and ultimately minimise the capital costs. The results must also be evaluated further from a process control perspective, to ensure ideal operating conditions which balance the benefits of vapour formation and prevent dry-out conditions. Overall, the So-St concept has the potential to become a sustainable low-emissions technology eliminating the reliance on the power plant steam cycle in carbon capture operations for cleaner energy production.

## ACKNOWLEDGMENT

The authors would like to thank the Department of Regional New South Wales for their financial support provided through the Coal Innovation New South Wales Fund (RDE493-30).

## REFERENCES

Aaron, D., & Tsouris, C. (2005). Separation of CO2 from flue gas: a review. *Separation Science and Technology, 40*(1-3), 321-348.

Abu-Zahra, M. R., Niederer, J. P., Feron, P. H., & Versteeg, G. F. (2007). CO2 capture from power plants: Part II. A parametric study of the economical performance based on mono-ethanolamine. *International Journal of Greenhouse Gas Control, 1*(2), 135-142.

Ben-Mansour, R., Habib, M., Bamidele, O., Basha, M., Qasem, N., Peedikakkal, A., Ali, M. (2016). Carbon capture by physical adsorption: materials, experimental investigations and numerical modeling and simulations–a review. *Applied energy, 161*, 225-255.

BP. (2020). Statistical Review of World Energy 2020.

Cheng, Z., He, Y., Cui, F., Xu, R., & Tao, Y. (2012). Numerical simulation of a parabolic trough solar collector with nonuniform solar flux conditions by coupling FVM and MCRT method. *Solar energy, 86*(6), 1770-1784.

Collier, J.G. & Thome J.R. (1994) Convective boiling and condensation. *Clarendon Press.*

Davis, J., & Rochelle, G. (2009). Thermal degradation of monoethanolamine at stripper conditions. *Energy Procedia, 1*(1), 327-333.

Duke, M. C., Ladewig, B., Smart, S., Rudolph, V., & da Costa, J. C. D. (2010). Assessment of postcombustion carbon capture technologies for power generation. *Frontiers of Chemical Engineering in China, 4*(2), 184-195.

Feron, P. H. (2009). The potential for improvement of the energy performance of pulverized coal fired power stations with post-combustion capture of carbon dioxide. *Energy Procedia, 1*(1), 1067-1074.

Figueres, C., Schellnhuber, H. J., Whiteman, G., Rockström, J., Hobley, A., & Rahmstorf, S. (2017). Three years to safeguard our climate. *Nature News, 546*(7660), 593.

IEA. (2013). Tracking clean energy progress 2013: IEA Publications Paris.

Kalogirou, S. A. (1996). Design of a solar low temperature steam generation system.

Khalilpour, R., Milani, D., Qadir, A., Chiesa, M., & Abbas, A. (2017). A novel process for direct solvent regeneration via solar thermal energy for carbon capture. *Renewable Energy, 104*, 60-75.

Khalilpour, R., Mumford, K., Zhai, H., Abbas, A., Stevens, G., & Rubin, E. S. (2015). Membrane-based carbon capture from flue gas: a review. *Journal of Cleaner Production, 103*, 286-300.

Kharangate, C. R., & Mudawar, I. (2017). Review of computational studies on boiling and condensation. *International Journal of Heat and Mass Transfer, 108*, 1164-1196.

Li, H., Yan, J., & Campana, P. E. (2012). Feasibility of integrating solar energy into a power plant with amine-based chemical absorption for CO2 capture. *International Journal of Greenhouse Gas Control, 9*, 272-280.

Lobón, D. H., Baglietto, E., Valenzuela, L., & Zarza, E. (2014a). Modeling direct steam generation in solar collectors with multiphase CFD. *Applied energy, 113*, 1338-1348.

Lobón, D. H., Valenzuela, L., & Baglietto, E. (2014b). Modeling the dynamics of the multiphase fluid in the parabolic-trough solar steam generating systems. *Energy Conversion and Management, 78*, 393-404.

Manzolini, G., Fernandez, E. S., Rezvani, S., Macchi, E., Goetheer, E., & Vlugt, T. (2015). Economic assessment of novel amine based CO2 capture technologies integrated in power plants based on European Benchmarking Task Force methodology. *Applied energy, 138*, 546-558.

Milani, D., Luu, M. T., Nelson, S., Liu, Y., Puxty, G., McNaughton, R., & Abbas, A. (2020a). Analysis for a solar stripper design for carbon capture under transient conditions. *International Journal of Heat and Mass Transfer, Under Review*.

Milani, D., Nelson, S., Luu, M. T., Meybodi, M. A., Puxty, G., & Abbas, A. (2020b). Tailored solar field and solvent storage for direct solvent regeneration: A novel approach to solarise carbon capture technology. *Applied Thermal Engineering*, 115119.

Moresa, P. L., Scennaab, N. J., & Mussatiab, S. (2011). Optimization Of A Stripper Unit For The Desorption Of MEA From (MEA-H2O-CO2) System.

Mumford, K. A., Wu, Y., Smith, K. H., & Stevens, G. W. (2015). Review of solvent based carbon-dioxide capture technologies. *Frontiers of Chemical Science and Engineering, 9*(2), 125-141.

Parvareh, F., Sharma, M., Qadir, A., Milani, D., Khalilpour, R., Chiesa, M., & Abbas, A. (2014). Integration of solar energy in coal-fired power plants retrofitted with carbon capture: A review. *Renewable & Sustainable Energy Reviews, 38*, 1029-1044. doi:10.1016/j.rser.2014.07.032

Qadir, A., Mokhtar, M., Khalilpour, R., Milani, D., Vassallo, A., Chiesa, M., & Abbas, A. (2013). Potential for solar-assisted post-combustion carbon capture in Australia. *Applied energy, 111*, 175-185.

Rubin, E., & De Coninck, H. (2005). IPCC special report on carbon dioxide capture and storage. *UK: Cambridge University Press. TNO (2004): Cost Curves for CO2 Storage, Part, 2*, 14.

Saghafifar, M., & Gabra, S. (2019). A critical overview of solar assisted carbon capture systems: Is solar always the solution? *International Journal of Greenhouse Gas Control*, 102852.

Sandeep, H., & Arunachala, U. (2017). Solar parabolic trough collectors: A review on heat transfer augmentation techniques. *Renewable and Sustainable Energy Reviews, 69*, 1218-1231.

Taylor, P. (2010). Energy Technology Perspectives 2010-Scenarios and Strategies to 2050. *International Energy Agency, Paris, France*.

Wibberley, L. (2010). Co2 capture using solar thermal energy: Google Patents.

Wilberforce, T., Baroutaji, A., Soudan, B., Al-Alami, A. H., & Olabi, A. G. (2019). Outlook of carbon capture technology and challenges. *Science of the Total Environment, 657*, 56-72.

Wilcox, D. C. (2008). Formulation of the kw turbulence model revisited. *AIAA journal, 46*(11), 2823-2838.

Yerdesh, Y., Belyayev, Y., Baiseitov, D., & Murugesan, M. (2018). Modeling two-phase flow in pipe of the solar collector. *International Journal of Mathematics and Physics, 9*(1), 12-19.

Yılmaz, İ. H., & Mwesigye, A. (2018). Modeling, simulation and performance analysis of parabolic trough solar collectors: A comprehensive review. *Applied energy, 225*, 135-174.

Zevenhoven, R., & Fagerlund, J. (2009). fixation by mineral matter; the potential of different mineralization routes.

Zhao, Y., Hong, H., Zhang, X., & Jin, H. (2012). Integrating mid-temperature solar heat and post-combustion CO2-capture in a coal-fired power plant. *Solar energy, 86*(11), 3196-3204.

## BIOGRAPHY

Scott Nelson is a fourth year undergraduate student studying a Bachelor of Engineering (Chemical and Biomolecular)/Bachelor of Science at the University of Sydney. He has received the Faculty of Engineering & IT Leadership Scholarship and is in his second year working as a Research Intern at CSIRO, supervised by Dr. Dia Milani. He is currently completing his Undergraduate Honours Thesis with supervisor Dr. Ali Abbas.